Renormalization of the electron-phonon coupling in the one-band Hubbard model

Erik Koch[1,2,*] and Roland Zeyher[1]

[1]*Max-Planck Institut für Festkörperforschung, Heisenbergstraße 1, 70569 Stuttgart, Germany*
[2]*Institut für Festkörperforschung, Forschungszentrum Jülich, 52425 Jülich, Germany*
(Received 17 March 2004; revised manuscript received 28 July 2004; published 21 September 2004)

We investigate the effect of electronic correlations on the coupling of electrons to Holstein phonons in the one-band Hubbard model. We calculate the static electron-phonon vertex within the linear response of Kotliar-Ruckenstein slave bosons in the paramagnetic saddle-point approximation. Within this approach the on-site Coulomb interaction U strongly suppresses the coupling to Holstein phonons at low temperatures. Moreover, the vertex function does *not* show particularly strong forward scattering. Going to larger temperatures $kT \sim t$ we find that after an initial decrease with U, the electron-phonon coupling starts to *increase* with U, confirming a recent result of Cerruti, Cappelluti, and Pietronero. We show that this behavior is related to an unusual reentrant behavior from a phase separated to a paramagnetic state upon *decreasing* the temperature.

I. INTRODUCTION

The relevance of phonons for high-temperature superconductivity has been debated since the discovery of the high-T_c cuprates. Superconductivity-induced changes in phonon frequencies which were observed in Raman[1] and inelastic neutron[2] scattering indicated dimensionless electron-phonon coupling strengths of the order of 10^{-2}. They thus pointed to a rather weak electron-phonon interaction in the cuprates. The rather large isotope effect on T_c in underdoped superconductors,[3] on the other hand, showed that the electron-phonon interaction cannot be neglected in a realistic theory for high-T_c superconductors. Recently, strong renormalization effects of the electrons near the Fermi surface, observed in angle-resolved photoemission spectroscopy (ARPES) in several cuprates, have been at least partially ascribed to phonons.[4,5] In agreement with this, ARPES measurements in underdoped $La_{2-x}Sr_xCuO_4$ revealed fine structure in the electron self-energy which has been associated with phonons.[6] Very spectacular are the recent discoveries of large oxygen isotope effects in the in-plane magnetic field penetration depth in several cuprates[7] and in the optical conductivity in $YBa_2Cu_3O_{6.9}$.[8] These effects clearly show that lattice properties may severely influence high-T_c superconductivity. One should, however, also note that the presence of these effects does not necessarily imply that the high-T_c superconductivity is caused by phonons.

The theoretical assessment of the role played by phonons in the cuprates involves two traditionally different topics. The first one concerns the magnitude of the bare electron-phonon coupling—i.e., the coupling in the absence of electronic correlations. In some approximation this bare coupling may be identified with the couplings deduced from band structure calculations in the local density approximation. Existing calculations[9,10] show that the strength of the bare electron-phonon coupling is weak or at most moderate and, in any case, too small to account for the observed T_c's within conventional Eliashberg theory or the observed kink feature in the electronic dispersion near the Fermi surface. The second topic to be addressed is the influence of strong electronic correlations on the above "bare" electron-phonon coupling and whether they enhance or suppress the bare couplings. Recent quantum Monte Carlo simulations of the Hubbard-Holstein model suggest that the electron-phonon coupling shows forward scattering and no substantial suppression at large U and small dopings,[11] similar as in the $1/N$ expansion for the t-J model.[12] On the other hand, it has been pointed out[13] that at small dopings the Kotliar-Ruckenstein (KR) slave-boson approach[14] might yield results quite different from the $1/N$ expansion. Taking correlation effects into account by means of exact diagonalization it has also been shown that the softening of the half-breathing phonon mode due to doping can be understood within the t-J model.[15] Nevertheless, the basic question whether electronic correlations enhance or suppress bare electron-phonon couplings has not yet been answered in a satisfactory way. Below we study the influence of strong electronic correlations on the electron-phonon coupling using the KR approach. The quantity of interest is the static vertex function Γ which acts as a momentum-dependent, multiplicative renormalization factor for the bare electron-phonon coupling.

II. METHOD

We consider the one-band Hubbard model on a square lattice with nearest- and next-nearest-neighbor hopping t and t', respectively:

$$H = -t \sum_{\langle i,j \rangle, \sigma} c_{j\sigma}^\dagger c_{i\sigma} - t' \sum_{\langle\langle i,j \rangle\rangle, \sigma} c_{j\sigma}^\dagger c_{i\sigma} + U \sum_i n_{i\uparrow} n_{i\downarrow}. \quad (1)$$

For the noninteracting system the dispersion relation is

$$\varepsilon_k = -2t[\cos(k_x) + \cos(k_y)] - 4t' \cos(k_x)\cos(k_y), \quad (2)$$

and the density of states has a logarithmic Van Hove singularity at $4t'$. For this model we want to study the influence of electronic correlations on the coupling of
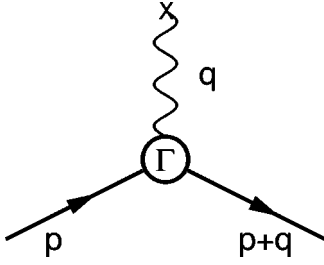
FIG. 1. Electron-phonon vertex within the linear response: The thick solid lines are the dressed propagators of the Hubbard model (1). The wavy line denotes the phonon—considered as a static external field as in $H_{\text{el-ph}}$.

electrons to an external field V_i. The bare coupling has the form

$$H' = \sum_{i,\sigma} n_{i\sigma} V_i. \qquad (3)$$

Writing $V_i = g u_i$, H' describes also the interaction of electrons and atomic displacements u_i with coupling constant g. An on-site coupling of this type has been found to be the strongest for a CuO_2 plane.[15]

The linear change in the one-particle Green's function $G(p)$ due to V_q is

$$\frac{\delta G(p)}{\delta V_q} = G(p)\Gamma(p,q)G(p+q), \qquad (4)$$

with the charge- or electron-phonon vertex

$$\Gamma(p,q) = -\frac{\delta G^{-1}(p)}{\delta V_q}. \qquad (5)$$

The components of the three-dimensional vectors p and q consist of a frequency and a two-dimensional momentum. For the calculation of the vertex we use the slave-boson technique of Kotliar and Ruckenstein.[14] The basic idea of our approach[16] is to calculate linear responses by linearizing the saddle-point equations for the perturbed system about the homogeneous saddle-point solution. We consider only paramagnetic solutions. Then there are three slave-bosons e, p, and d describing empty, singly, and doubly occupied sites and two Lagrange parameters $\lambda^{(1)}$ and $\lambda^{(2)}$ enforcing consistency between slave fermions and slave bosons. The linear response to a chargelike perturbation of a given wave vector can be determined by solving the 5×5 system of linear equations. With the notation of Ref. 16 the static charge susceptibility for wave vector $\mathbf{q}$ is then given by

$$\chi(\mathbf{q}) = \frac{\delta n_{\mathbf{q}}}{\delta V_{\mathbf{q}}} = 4\left(p\frac{\delta p}{\delta V_{\mathbf{q}}} + d\frac{\delta d}{\delta V_{\mathbf{q}}}\right) \qquad (6)$$

and the static electron-phonon vertex function (Fig. 1) for an electron with incoming momentum $\mathbf{p}$ and an external phonon of wave vector $\mathbf{q}$ by

$$\Gamma(\mathbf{p},\mathbf{q}) = 1 + \frac{\delta\lambda^{(2)}}{\delta V_{\mathbf{q}}} + z(\varepsilon_{\mathbf{p}} + \varepsilon_{\mathbf{p+q}})\frac{\delta z}{\delta V_{\mathbf{q}}}, \qquad (7)$$

with

$$\frac{\delta z}{\delta V_{\mathbf{q}}} = \frac{\partial z}{\partial e}\frac{\delta e}{\delta V_{\mathbf{q}}} + \frac{\partial z}{\partial p}\frac{\delta p}{\delta V_{\mathbf{q}}} + \frac{\partial z}{\partial d}\frac{\delta d}{\delta V_{\mathbf{q}}}, \qquad (8)$$

$V_{\mathbf{q}}$ the static external field, and z given by the Kotliar-Ruckenstein choice

$$z = \frac{(e+d)p}{\sqrt{1-p^2-d^2}\sqrt{1-e^2-p^2}}. \qquad (9)$$

The first term in Eq. (7) is due to the explicit dependence of G^{-1} on V; the remaining terms are obtained by taking the derivative of the self-energy with respect to V and reflect the changes in the boson variables in response to the external perturbation. Γ does not depend on frequencies because we assumed zero frequency in q and because the saddle-point self-energy is frequency-independent.

In the limit $U \to \infty$ our approach reduces to method (II) of Ref. 13, and we have checked that for large U we recover the results given in their Fig. 1.

III. CHECKS

While it was shown that the slave-boson linear-response method gives very good results for the charge susceptibility (see, e.g., Fig. 1 of Ref. 16 for a comparison with exact diagonalization), it is not clear *a priori* how well it will work for the charge vertex $\Gamma(\mathbf{p},\mathbf{q})$. As a check we have calculated the static vertex for a small system using exact diagonalization. The result for the scattering of an electron from a state just below to a state just above the Fermi surface is shown in Fig. 2. Considering the fact that in exact diagonalization the number of particles is fixed, while the slave-boson calculations are performed in the grand canonical ensemble, the agreement between both methods is remarkably good. This indicates that the slave-boson approach should work well at zero temperature.

To find out how well the slave bosons work at finite temperatures we compare to the quantum Monte Carlo (QMC) calculations of Ref. 11. Figure 4 of that work shows the effective electron-phonon coupling $g(\mathbf{p},\mathbf{q})$, as defined in their Eq. (7), for the Hubbard model on an 8×8 lattice with filling $n = 0.88$, calculated at the lowest fermionic Matsubara frequency, for an inverse temperature of $\beta = 2$. For comparison, we show in Fig. 3 the results of our slave-boson calculations for the same model at $\omega = 0$ and a slightly different filling $n = 0.875$. The electrons have been put to the isoenergy line $\varepsilon_p = 0$ (noninteracting Fermi surface for half-filling). As follows from Eq. (7), the vertex in the slave-boson linear response is then independent of $\mathbf{p}$. Thus both plots in Fig. 4 of Ref. 11 can be compared to the curves shown above, disregarding slight differences in the fillings and in that the QMC calculations of Ref. 11 has not been done at $\omega = 0$. It is remarkable that the two quite different calculations yield very similar results. In particular, we find that after an initial decrease the coupling for forward
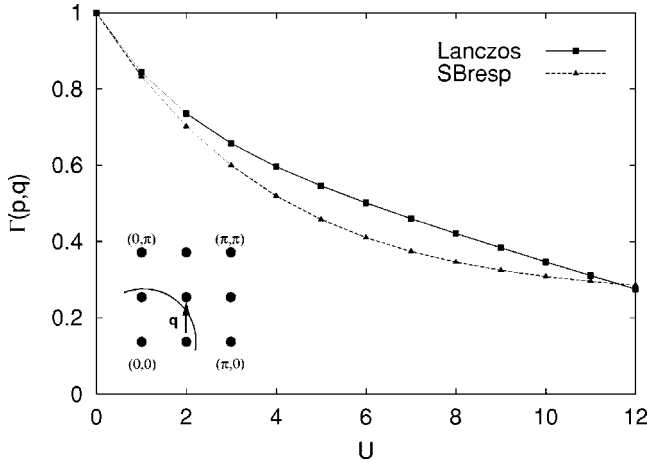
FIG. 2. Electron-phonon vertex $\Gamma(\mathbf{p},\mathbf{q})$ for the scattering of an electron with $\mathbf{p}=(\pi/2,0)$ by a static phonon of wave vector $\mathbf{q}=(0,\pi/2)$ (see inset, where the points denote the allowed $\mathbf{p}$ vectors and the solid line the Fermi line) for $t'=0$ on a 4×4 lattice with periodic boundary conditions and five up and five down electrons. The solid line gives the result of a Lanczos (with fixed number of electrons), the dashed line of a slave-boson calculation for the same lattice. The energy unit is t.

scattering (small $\mathbf{q}$) starts to *increase* for $U\gtrsim8$. This seems to indicate that the slave-boson method also works well at finite temperatures. Moreover, Eq. (7) naturally explains why the QMC results for different electron momenta $\mathbf{p}$, shown in Fig. 4 of Ref. 11, are so similar.

IV. ELECTRON-PHONON VERTEX

After comparing the results of the slave-boson linear response calculations to more accurate methods, which are, however, limited to small systems (exact diagonalization) or finite temperatures (quantum Monte Carlo), we now turn to very large systems at very low temperatures. First we calculate the electron-phonon vertex for electrons on the Fermi surface, where in Eq. (7) $\varepsilon_\mathbf{p}$ and $\varepsilon_{\mathbf{p}+\mathbf{q}}$ are
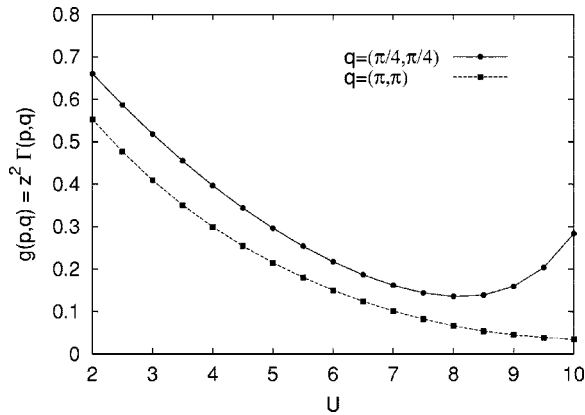

FIG. 3. Effective electron-phonon coupling for $t'=0$ on an 8×8 lattice with filling $n=0.875$ (28+28 electrons) as calculated in slave-boson linear response at an inverse temperature of $\beta=2$ and for electron momenta on the line $\varepsilon_p=0$.
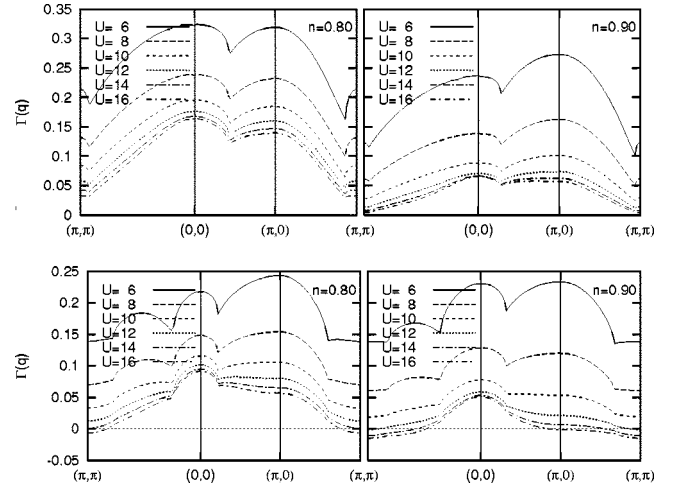

FIG. 4. Electron-photon vertex $\Gamma(\mathbf{q})$ for scattering electrons on the Fermi surface. Calculations are for $t'=0$ (top) and $t'=-0.35t$ (bottom), an inverse temperature $\beta=500/t$, and different fillings n.

both replaced by the Fermi energy of the noninteracting system. As a result, the vertex becomes independent of the electron momentum $\mathbf{p}$ and in the following will therefore be denoted simply by $\Gamma(\mathbf{q})$. Figure 4 shows the vertex for momentum transfer $\mathbf{q}$ along high-symmetry lines in the Brillouin zone for the Hubbard model at essentially zero temperature. The effect of next-nearest-neighbor hopping is illustrated by comparing calculations for $t'=0$ and $t'=-0.35t$. We find that in both cases the on-site Coulomb interaction strongly reduces the electron-phonon coupling. The reduction is monotonic with increasing U and for large values eventually reaches $\lim_{U\to\infty}\Gamma(\mathbf{q})$. This behavior is not completely unexpected as the charge response should be strongly suppressed by an on-site Coulomb interaction. It is, however, in striking difference to the behavior at higher temperature (Fig. 3). Also, while $\Gamma(\mathbf{q})$ shows a broad peak around $\mathbf{q}=0$, we do not find a particularly pronounced forward scattering. In fact, the electron-phonon vertex is often strongest close to $\mathbf{q}=(\pi,0)$. This is different from what was found within an $1/N$ expansion.[12] The $1/N$ expansion relies on the smallness of $1/\delta N$; i.e., it breaks down at small dopings $\delta=1-n$. This can be seen from the fact that the charge-charge correlation function remains in leading order finite for $\delta\to0$ though the exact correlation function vanishes in this limit. The Kotliar-Ruckenstein method, on the other hand, reproduces this limit correctly in leading order which makes it plausible that in this case the charge vertex is smaller than in the $1/N$ expansion, especially at smaller dopings.[13] Which of the two methods is more reliable, in particular, near optimal doping, is not clear and can probably only be judged by comparison with exact numerical methods.

V. EFFECTIVE COUPLING CONSTANTS

To assess the importance of the electron-phonon coupling for superconductivity we calculate the renormalization factor
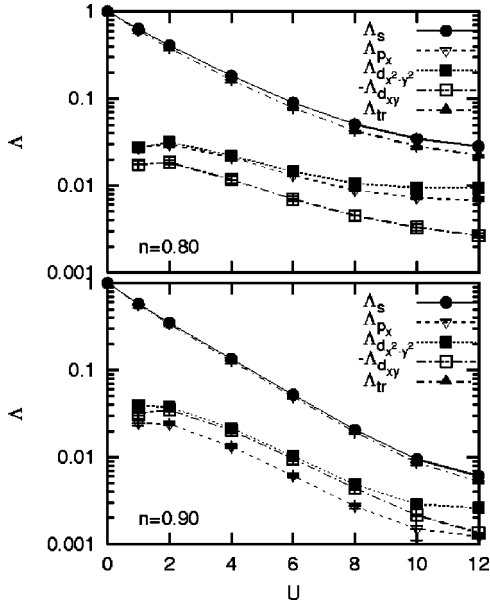
FIG. 5. Renormalization constants Λ_α for $t'=0$ and different symmetry channels and for Λ_{tr} relevant for transport.

$$\Lambda_\alpha = \frac{\int_{FS} \frac{dp}{|\mathbf{v_p}|} \int_{FS} \frac{dp'}{|\mathbf{v_{p'}}|} g_\alpha(\mathbf{p}) \Gamma(\mathbf{p}, \mathbf{p'} - \mathbf{p}) g_\alpha(\mathbf{p'})}{z^2 \int_{FS} \frac{dp}{|\mathbf{v_p}|} \int_{FS} \frac{dp'}{|\mathbf{v_{p'}}|} g_\alpha^2(\mathbf{p})}$$

for the symmetry channels

$$g_s(\mathbf{p}) = 1,$$

$$g_{s*}(\mathbf{p}) = \cos(p_x) + \cos(p_y),$$

$$g_{p_x}(\mathbf{p}) = \sin(p_x),$$

$$g_{d_{x^2-y^2}}(\mathbf{p}) = \cos(p_x) - \cos(p_y),$$

$$g_{d_{xy}}(\mathbf{p}) = \sin(p_x)\sin(p_y).$$

Λ_α is equal to the ratio $\lambda_\alpha / \lambda_\alpha^{(0)}$, where λ_α and $\lambda_\alpha^{(0)}$ denote the dimensionless electron-phonon coupling constants in the interacting and noninteracting cases, respectively. To judge the importance of forward scattering we also calculate the renormalization factor for transport:

$$\Lambda_{tr} = \frac{\int_{FS} \frac{dp}{|\mathbf{v_p}|} \int_{FS} \frac{dp'}{|\mathbf{v_{p'}}|} \Gamma(\mathbf{p}, \mathbf{p'} - \mathbf{p}) |\mathbf{v}(\mathbf{p}) - \mathbf{v}(\mathbf{p'})|^2}{2z^2 \int_{FS} \frac{dp}{|\mathbf{v_p}|} \int_{FS} \frac{dp'}{|\mathbf{v_{p'}}|} |\mathbf{v}(\mathbf{p})|^2}.$$

The results are shown in Fig. 5. Calculations were performed for lattices of increasing size at decreasing temperatures, performing the $\mathbf{p}$ integrals over the whole Brillouin zone and weighting with a minus sign the derivative of the Fermi-Dirac distribution $-f'(\varepsilon_p) = \beta f(\varepsilon_p)[1 - f(\varepsilon_p)]$, which becomes a δ function for $T=0$. Convergence of the $T \to 0$ extrapola-
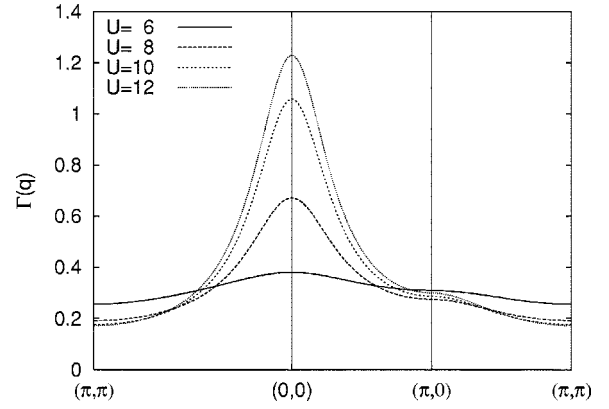

FIG. 6. Electron-phonon vertex $\Gamma(\mathbf{q})$ for scattering on the Fermi surface. Calculations are for $t'=0$, filling $n=0.80$, and an inverse temperature $\beta=1$.

tion has been checked by comparing Λ_s and Λ_{s*}, which only for $T=0$ are equal. Error bars for the extrapolation are plotted, but are usually smaller than the size of the plotting symbols.

We find that for $U \lesssim 10$ the s-wave couplings decrease almost exponentially with U. For the special case of the Hubbard model with nearest-neighbor hopping only ($t'=0$) we have $\Lambda_s^* = \Lambda_s$, since g_{s*} is constant on the Fermi surface. Moreover, $\Lambda_{tr} \approx \Lambda_s$, reflecting that there is no pronounced forward scattering; only for larger U does Λ_{tr} become somewhat smaller than Λ_s. But by then both coupling constants are already very small. The higher-symmetry channels are even weaker. Since $\Gamma(\mathbf{q}) \equiv 1$ for $U=0$, they vanish for $U=0$ by symmetry, then go through a maximum around $U=2$, only to decay almost exponentially. We can thus conclude that within Kotliar-Ruckenstein slave-boson theory, restricting the system to be paramagnetic, the contribution of Holstein phonons to superconductivity should be very small.

VI. PHASE SEPARATION

We now come back to the surprising upturn of the electron-phonon vertex for $U \gtrsim 8$ shown in Fig. 3 and also found in the QMC calculations of Ref. 11. Calculating $\Gamma(\mathbf{q})$ at $kT \sim t$, we indeed find a drastically different behavior than for $T \to 0$: Instead of monotonically decreasing with U, the coupling starts to *increase* and develops a very strong forward scattering peak. An example is shown in Fig. 6. The calculated curves should be compared to the uppermost panel on the right of Fig. 4. Looking at the charge response function $\chi(\mathbf{q})$ in the paramagnetic phase we find that this behavior is a precursor of a phase-separation instability—a divergence of $\chi(\mathbf{q}=0)$. This has also been pointed out in Ref. 17. Calculating the phase diagram, we find a very peculiar reentrant behavior around the phase separated region for finite U as shown in Fig. 7: When cooling down the system phase separates, but at low enough temperature it reverts back to the paramagnetic phase.

The occurrence of phase separation can be studied in a simple way directly from the grand canonical potential for
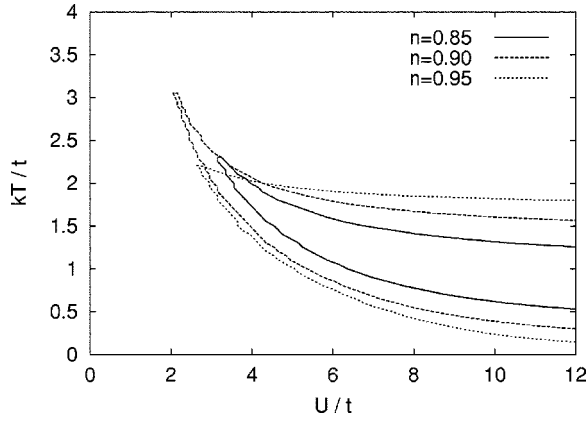
FIG. 7. Phase separation in the Hubbard model with $t'=0$: the lines enclose the region where the paramagnetic slave-boson saddle-point solution is unstable against phase separation. For $t'/t>0$ the region of phase separation tends to increase; for $t'/t<0$ it tends to decrease, in particular, for large doping.

the paramagnetic phase: The density n is then given by minus the derivative of the grand canonical potential density with respect to the chemical potential μ:

$$n = 2 \int_{-\infty}^{\infty} \frac{d\epsilon \rho(\epsilon)}{e^{\beta(z^2\epsilon-\tilde{\mu})} + 1},\qquad(10)$$

where $\rho(\epsilon)$ denotes the density of states of the noninteracting system. We consider the limit $U \to \infty$, where z^2 is given by $(1-n)/(1-n/2)$ and $\tilde{\mu}$ by $\mu+E/(1-n/2)^2/2$. Here E is the average kinetic energy given by Eq. (10) with an additional factor ϵ in the integrand. For fixed n, Eq. (10) can be solved first as a function of $\tilde{\mu}$ and then of μ. Figure 8 shows numerical results for $\mu(n)$ for the dispersion of Eq. (2) with $t'=0$ at six different temperatures. For large temperature $\mu(n)$ is a monotonically increasing function and the system is stable. For $kT \lesssim 2t$ the slope of $\mu(n)$ becomes negative close to half-filling, indicating phase separation. For a finite but large U, μ increases steeply with increasing n for $n>1$. Taking the limit $U \to \infty$ this part of the curve collapses onto the entire positive vertical axis at $n=1$. In the phase-separated region three different densities belong then to one value of the chemical potential. The usual Maxwell construction can then be applied showing that one component in the phase-separated region is always half-filled. Calculating the slope of $\mu(n)$ at $n=1$ we find

$$\lim_{n\nearrow1}\frac{d\mu}{dn} = \frac{2}{\beta}(1 - \rho_2\beta^2),\qquad(11)$$

where ρ_2 is the second moment of the density of states, which in the present case is equal to $4t^2$. Thus, for the square lattice with $t'=0$ there is phase separation for $kT<2t$ and, unlike the case of finite U, there is no reentrance of the homogeneous phase. The numerically determined curves in Figs. 7 and 8 are compatible with this exact value.

Since in our calculations we only allow for a paramagnetic phase, other phases might mask the phase separation. Also, since slave bosons may have problems at high
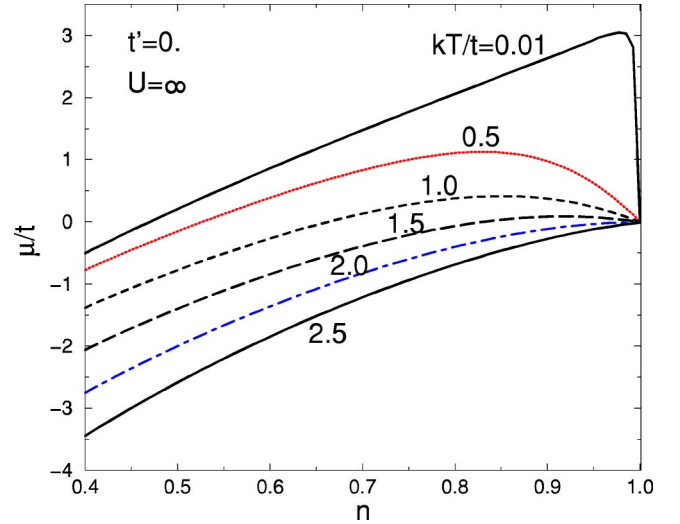

FIG. 8. Dependence of the bare chemical potential μ on n for $t'=0$ and $U=\infty$. Phase separation occurs if the slope of $\mu(n)$ is negative. Note that in the limit $U\to\infty$ the $\mu(n)$ curve for $n>1$ collapses onto the entire positive vertical axis at $n=1$ so that the usual Maxwell construction can be applied.

temperatures,[14] it is not clear if the Hubbard model really shows such a reentrant behavior. Nevertheless, we find a qualitatively similar behavior in the limit $U\to\infty$ in the gauge- invariant $1/N$ expansion (i.e., a theory without Bose condensation).

Phase separation at finite T has also been proposed in Refs. 18–20. Moreover, the good agreement with the quantum Monte Carlo calculations of Ref. 11 suggests that our approach might indeed capture the relevant physics. It would therefore be interesting to test the phase diagram shown in Fig. 7 with QMC: A calculation for, e.g., $\beta=1$ and $U=4,\dots,8$—i.e., at temperatures and values of U, where QMC has little problems—should show clear signs of phase separation. Of course, these calculations should be done at $\omega=0$ as the extrapolation from finite Matsubara frequencies might be difficult close to an instability.

VII. CONCLUSIONS

In conclusion, we have studied the influence of strong electronic correlations on the electron-phonon interaction for the Hubbard-Holstein model using the Kotliar-Ruckenstein slave-boson method. For high temperatures the boundaries of the phase-separated state were determined in the T-U plane for different dopings and the increase of the static vertex Γ near the boundaries was studied, confirming and extending recent results of Ref. 17. At low temperatures and moderate or small dopings we found that Γ does not exhibit pronounced forward scattering behavior and that Γ reduces dramatically the electron-phonon coupling. It seems that exact numerical calculations are necessary to judge the reliability of the $1/N$ and the Kotliar-Ruckenstein approaches.

ACKNOWLEDGMENTS

*Electronic address: E.Koch@fz-juelich.de

[1] C. Thomsen and M. Cardona, in *Physical Properties of High-Temperature Superconductors I*, edited by D.M. Ginzberg (World Scientific, Singapore, 1989), p. 409.

[2] D. Reznik, B. Keimer, F. Dogan, and I.A. Aksay, Phys. Rev. Lett. **75**, 2396 (1995).

[3] J.P. Frank, in *Physical Properties of High-Temperature Superconductors IV*, edited by D.M. Ginzberg (World Scientific, Singapore, 1994), p. 189.

[4] A. Lanzara, P.V. Bogdanov, X.J. Zhou, S.A. Kellar, D.L. Feng, E.D. Lu, T. Yoshida, H. Eisaki, A. Fujimori, K. Kishio, J.-I. Shimoyoama, T. Noda, S. Uchida, Z. Hussain, and Z.-X. Shen, Nature (London) **412**, 510 (2001).

[5] R. Zeyher and A. Greco, Phys. Rev. B **64**, 140510 (2001).

[6] X.J. Zhou *et al.*, cond-mat/0405130 (unpublished).

[7] R. Khasanov, D.G. Eshchenko, H. Luetkens, E. Morenzoni, T. Prokscha, A. Suter, N. Garifianov, M. Mali, J. Roos, K. Conder, and H. Keller, Phys. Rev. Lett. **92**, 057602 (2004).

[8] C. Bernhard, T. Holden, A.V. Boris, N.N. Kovaleva, A.V. Pimenov, J. Humlicek, C. Ulrich, C.T. Lin, and J.T. Tallon, Phys. Rev. B **69**, 052502 (2004).

[9] O. Jepsen, O.K. Andersen, I. Dasgupta, and S. Savrasov, J. Phys. Chem. Solids **59**, 1718 (1998).

[10] K.-P. Bohnen, R. Heide, and M. Krauss, Europhys. Lett. **64**, 104 (2003).

[11] Z.B. Huang, W. Hanke, E. Arrigoni, and D.J. Scalapino, Phys. Rev. B **68**, 220507(R) (2003).

[12] M.L. Kulić and R. Zeyher, Phys. Rev. B **49**, 4395 (1994); R. Zeyher and M.L. Kulić, *ibid.* **53**, 2850 (1996).

[13] J. Keller, C.E. Leal, and F. Forsthofer, Physica B **206&207**, 739 (1995).

[14] G. Kotliar and A.E. Ruckenstein, Phys. Rev. Lett. **57**, 1362 (1986).

[15] O. Rösch and O. Gunnarsson, Phys. Rev. Lett. **92**, 146403 (2004).

[16] E. Koch, Phys. Rev. B **64**, 165113 (2001).

[17] E. Cappelluti, B. Cerruti, and L. Pietronero, Phys. Rev. B **69**, 161101(R) (2004).

[18] P. Wölfle, J. Low Temp. Phys. **99**, 625 (1995).

[19] S. Onoda and M. Imada, J. Magn. Magn. Mater. **272–276**, 275 (2004).

[20] E. Cappelluti and R. Zeyher, Phys. Rev. B **59**, 6475 (1999).